Contract No:

This document was prepared in conjunction with work accomplished under Contract No. 89303321CEM000080 with the U.S. Department of Energy (DOE) Office of Environmental Management (EM).

Disclaimer:

A FRAMEWORK WITH EXAMPLES FOR PRINTING THERMOSETTING POLYMERS USING LASER POWDER BED FUSION ADDITIVE MANUFACTURING

C. A. Chatham[1] and A. L. Washington II[2]

[1] Advanced Engineering Division, Savannah River National Laboratory, Aiken, SC 29808
[2] Advanced and Energy Materials, Savannah River National Laboratory, Aiken, SC 29808

Abstract

Thermoset polymers possess traits arising from their covalently crosslinked network structure that are distinct from thermoplastic polymers. These traits can manifest as relative increases in the performance properties of chemical resistance, stiffness, and strength particularly at elevated temperature. Although these performance properties are desired from additively manufactured parts, there are few engineering grade thermosetting polymers commercially available for any additive manufacturing (AM) fabrication method. This work describes some of the challenges when processing and formulating thermosetting powder feedstocks for the laser powder bed fusion (L-PBF) mode of AM. The thermal curing properties of three different commercially available thermosetting polymers made via L-PBF are compared. Surface temperature profiles collected during printing are used to predict the extent of crosslinking through a rudimentary isoconversional model and are compared against post-print measurements of residual cure.

Introduction

Many industries continue to increase their implementation of additive manufacturing (AM) technologies as layerwise fabrication transitions from primarily prototyping applications towards manufacturing of end-use parts. Of the seven technology categories identified by ISO/ASTM 52900 [1], powder bed fusion (PBF) is often championed for end-use production due to its batch-style fabrication, large build size, and low anisotropy compared to other AM processes [2, 3]. Additionally, the materials commercially available for PBF currently include relevant engineering grade polymers, like nylon and PEKK [4]. However, no one family of materials is adequate for every application. Certain applications demand a stiff mechanical performance even at elevated temperatures and in the presence of harsh solvents. Traditionally, these performance properties are associated with crosslinked network polymers, which are not currently commercially available for use in PBF AM.

The defining characteristic of PBF AM as described in ISO/ASTM 52900:2021 is “thermal energy selectively fusing” specific regions of a powder bed in a layerwise manner to fabricate a 3D part [1]. When that energy is supplied via a scanning laser, the technology is termed laser-powder bed fusion (L-PBF). Due to its nature as a thermal process with solid powder-form feedstock, L-PBF is most often used to process thermoplastic polymers. Recent review papers that provide an overview of materials printed via L-PBF AM do not include any thermosetting polymers and often specifically describe how the heat-and-reform style manufacturing process lends itself to thermoplastic polymers [4, 2, 3, 5]. What little published literature exists for L-PBF

of thermosets can be categorized by the point in the manufacturing process relative to the printing step when the network structure is formed. The following paragraphs summarize published literature for thermoset parts made using L-PBF that form the covalent network structure either (i) pre-printing or (ii) post-printing.

Covalent adaptable networks (CAN) are one way to form a network structure pre-print. CANs of poly(dimethyl siloxane) (PDMS) has been demonstrated printable via laser powder bed fusion (L-PBF) by Sun, et al. [6]. Sun, et al. demonstrated the useful self-healing and elastomeric properties of CANs for a shoe insole application. According to their report, the PDMS CAN pre-existed L-PBF processing then was broken and reformed during printing and again in the form of a printed part to showcase its "self-healing" performance. Although CANs are covalently crosslinked networks at application temperatures, the network is broken at processing temperatures resulting in thermoplastic-like processing behavior. Such polymers do not require the additional considerations of curing while printing. Additionally, the same researchers have reported L-PBF printing a polyurethane with a dynamic covalent bond based on the Diels-Alder reaction [7]. They report dramatically decreased anisotropy in printed CANs. The improved z-direction tensile strength is claimed to be a result of forming dynamic crosslinks across layer boundaries. [7]

The second general method for L-PBF of thermosetting polymers is forming the network post-printing. Researchers from NASA report their initial and revised printing efforts for their target aerospace grade polyimides [8, 9]. Using their method, an uncrosslinked, near-net shape "green part" is prepared using a DTM Sinterstation L-PBF machine (λ = 10.6 μm) before crosslinking the chain-ends during a 16 h post-print thermal bake. Published work by Hassan, et al. and Campbell, et al. employ similar approaches. Hassan and coauthors use a Sinterit Lisa (λ = 808 nm) to make a bismaleimide green body followed by a 61 h thermal post-process at various isothermal steps [10]. Campbell, et al. report printing a two-part epoxide plus amino sulfone green part with a Sintratec Kit (λ = 455 nm) prior to crosslinking the chain-ends during an 85 h post-print thermal bake [11].

Separating the steps of macro-scale geometry formation and micro-scale polymer network formation have distinct advantages noted by authors of each prior work. Specifically, the heating environment and rheology can be tailored to the activity of interest. A mismatch between heating, flow, and curing may cause significant geometric distortion when attempting to thermally cure freestanding objects. Partially pre-reacting polymer systems provides appropriate green-part strength so that fused parts can hold shape during post-printing cure cycles. Additionally, Chung, et al.'s reported cure cycles for their polyimide involved lengthy, stepwise heating to ensure geometric stability as the crosslinked network was slowly formed in the free-standing green body [9]. Campbell, et al. discuss the importance of slow curing kinetics to avoid shape distortion [11].

Note that the logical third category of forming a covalently crosslinked network during printing is absent from published literature. The present work described in this paper contributes towards closing that knowledge gap. In the present work, the authors describe translating commercial off-the-shelf (COTS) oven-cure thermosetting polymers into the local, rapid, and cyclic laser heating environment of L-PBF AM. The discussion centers on the predicting extent of cure from *in situ* temperature profiles collected with an IR camera and comparing predicted values against post-print measurements. The authors conclude by synthesizing observations into guidelines and an early outlook on forming network polymers during L-PBF AM.

Materials and Methods

Thermosetting Materials. One of the most challenging requirements for L-PBF AM is the spherical particle feedstock form. Most polymer L-PBF powders have an average particle diameter between 45-90 µm with a narrow overall distribution between 20-120 µm and are required to be very spherical [2]. Powder paint is one current, commercial application that uses powdered thermosetting polymer precursors; therefore, the following three COTS powder paints were used in this study: Vulcan Black (TGIC-containing polyester) by Axalta, Oil Black (epoxy-based) by Axalta, and the TD 61 series Anodized Effect (TGIC-free polyester) from TIGER Drylac. These materials span three different curing reactions providing multiple crosslink pathways to evaluate in the rapidly cyclic heating environment of L-PBF.

Manufacturing Methods. All specimens prepared for this work were made using a Sintratec Kit L-PBF additive manufacturing machine (λ = 455 nm), which operates in air. The researchers determined suitable fabrication settings on the Sintratec Kit from previous experimentation to ensure complete and viable parts would be fabricated. These parameters are included in Table 1. OEM recommended isothermal oven cure times are included in SI TABLE 1 as a point of reference.

Table 1. Printing parameters used for each material.

Material	Chamber Temperature [°C]	Powder Surface Temperature [°C]	Beam Speed [mm s^{-1}]	Layer Height [µm]	Hatch Spacing [µm]	Number of Perimeters	Perimeter offset [µm]
Vulcan Black (TGIC Polyester)	70	50	20, 40, 60	120	80	10	1
Oil Black (Epoxy)	70	50	20, 40, 60	120	80	10	1
TD 61 (TGIC free polyester)	70	50	20, 40, 60, 150, 235	120	80	10	1

A FLIR X6901SC thermal imaging camera was used to determine the affected maximum temperature and resultant temperature decay profile from the chosen print parameter combination for each material. The camera was mounted adjacent to the Sintratec Kit to look through the FLIR Series 4 broadband crystal view port onto the powder bed. As all three tested powders are black, they were assumed to have an emissivity of 0.95. Nine regions of interest were defined around a grid of printed cylinders. A representative image is shown in Figure 1.

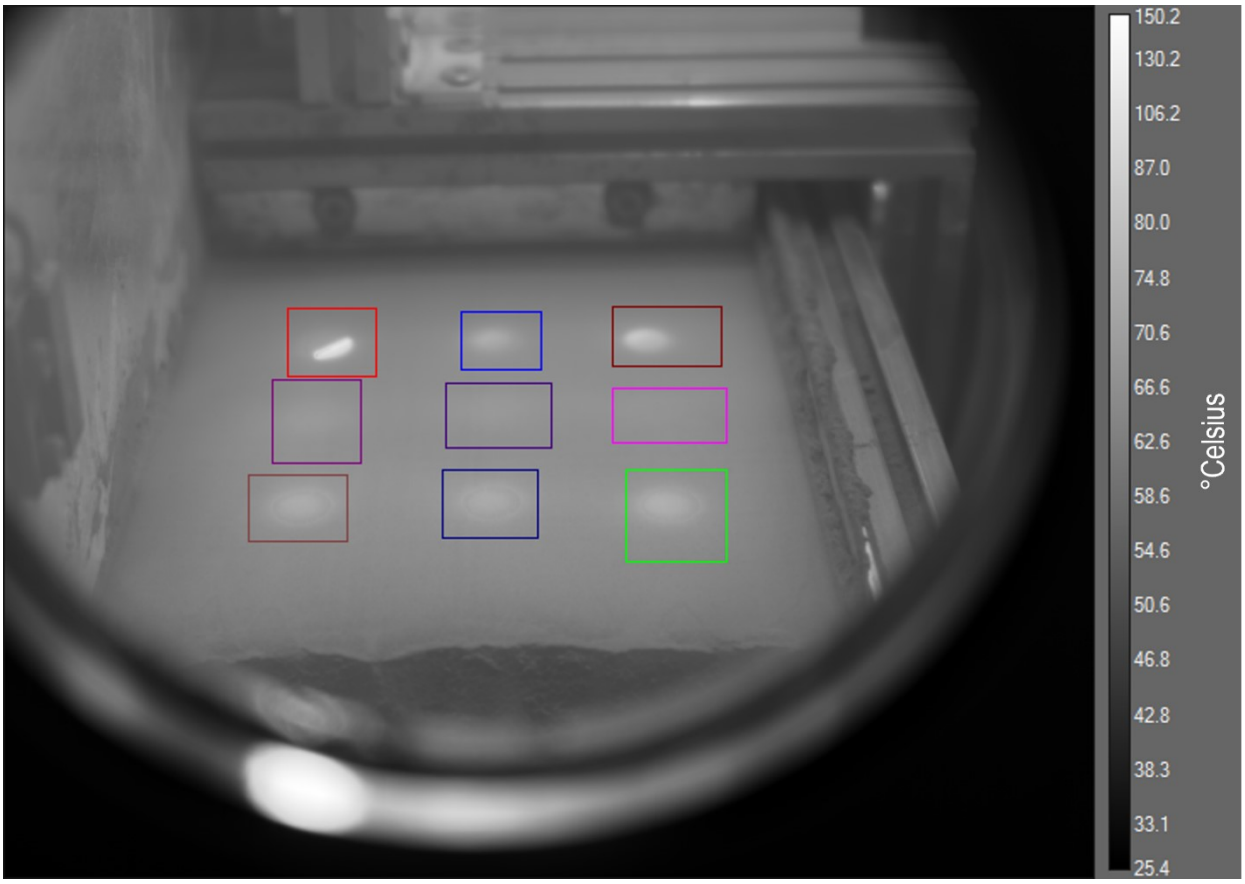

Figure 1. Representative image of field of view for FLIR camera *in situ* temperature measurements. Each region of interest captures the maximum temperature of the circular cross-section of the printed cylinder. The grayscale image correlates to temperature readings in Celsius.

Differential Scanning Calorimetry (DSC). Samples of powdered feedstock were run on a Mettler Toledo DSC 3+ unit using heating rates of 3, 5, 10, and 20 °C min^{-1}. Test temperature ranges were varied by component material but were conducted to provide at least 25 °C of baseline measurement before and after observed phase transitions and curing reactions. Data analysis to integrate underneath the exothermic curing peaks and generate extent of reaction as functions of time and temperature was performed using the Mettler Toledo STARe software.

Samples of printed parts were run on the same Mettler Toledo DSC 3+ unit at a heating rate of 10 °C min^{-1} to determine the residual cure. Complete cure (ΔH_x^0) was taken to be the average of heat evolved during crosslinking of powdered feedstock from three replicate specimens at 10 °C min^{-1}. The heat evolved over a similar temperature range in the printed parts ($\Delta H_{x,s}$) was determined and normalized to ΔH_x^0. This ratio is "residual cure;" one minus the ratio is "extent of cure."

Isoconversional Analysis. Isoconversional analysis was performed on DSC data using both Microsoft Excel and custom Python scripts. Data were extracted using Excel to the tabular form relating time, temperature, and integrated energy information to percent conversion. Both

linear (Excel) and non-linear (Python; Spyder IDE; SciPy curve_fit()) methods were used in combination to determine key kinetic information (i.e., activation energy and rate of reaction) of each material. Linear fitting to determine activation energy was performed via Kissinger method, shown in Equation 1 In the equation, β is the heating rate, T_p is the absolute temperature at maximum rate of reaction, E is activation energy, and R is the ideal gas constant (8.314 J mol^{-1} K^{-1}).

$$ln\left(\frac{\beta}{T_p^2}\right) = \frac{-E}{R}\left(\frac{1}{T_p}\right) \quad \text{Equation 1}$$

Non-linear curve-fitting to determine model parameters A, m, and n was performed via Equation 2, similar to the procedure described in Reference [12]. In this equation, α is extent of reaction.

$$\ln\left(\beta\frac{d\alpha}{dT}\right) + \frac{E_A}{RT} = \ln(A) + m * \ln(\alpha) + n * \ln(1-\alpha) \quad \text{Equation 2}$$

Intermediate results for linear curve fits and validation plots for non-linear curve fits are included as part of Supplemental Information.

Adaptation of Process Parameter Bounding Theory for Thermosetting Polymers

Published research and discussion detailing process parameter value selection for thermoplastic polymers is often centered around the energy melt ratio (EMR) and EMR for degradation first put forward by Starr, et al. [13] and Vasquez, et al. [14] in their work with nylon-12. Chatham, et al., rearranged and expanded the EMR (Equation 3 below; Equation 3 from [15]) in a manner to predict minimum and maximum laser power values for their work processing poly(phenylene sulfide) [15]. This works further adapts that equation for the case of a reactive polymer.

$$P_{min} = \frac{h \times V_b \times l}{SC}\left(\left[C_p \times (T_m - T_b) + \Delta H_m\right] \times Q \times \Phi\right) \quad \text{Equation 3}$$

In Equation 3 P_{min} is the minimum power required to achieve full melting of a unit volume of powder material with the standard process parameters of hatch spacing (h), beam speed (V_b), layer height (l), and scan count (SC). The equation describes a material of density Q, powder packing fraction Φ, and specific heat C_p, being heated from the bed temperature T_b to the polymer's melting temperature T_m. To achieve full melting, the latent heat of melting ΔH_m must also be overcome.

To adapt prior work that focused on the purely physical, thermoplastic process to the case of reactive polymers, we will address the following additional topics: (1) reaction activation energy and (2) temperature dependent reaction rate. As these concerns are specific to encouraging chemical reactions during L-PBF, this new, adapted form of the EMR will be referred to as the Energy Reaction Ratio, "EXR."

Additional Concern 1: Reaction Activation Energy. For the case of materials that undergo a reaction in their melt state, we add the activation energy for the reaction to occur E_{Ax} at temperature T_x, as shown in Equation 4. For the present work, we assume that the onset of crosslinking occurs at a temperature higher than the end of melting (i.e., $T_x > T_m$).

$P_{min} = \frac{h \times V_b \times l}{SC}\left(\left[C_p \times (T_x - T_b) + \Delta H_m + E_{Ax}\right] \times Q \times \Phi\right)$	Equation 4

Although crosslinking is an exothermic reaction and will be expected to locally raise the temperature, it is not included in Equation 4 because this would artificially decrease the required power predicted since the printer must first overcome E_A before that energy is released.

Additional Concern 2: Kinetic Maxima. When processing semi-crystalline thermoplastic polymers, the goal is to reach a fully molten state to encourage rapid coalescence. This is most reliably achieved by raising the temperature above the equilibrium melting temperature, T_m^0. In this way, the melting phenomenon follows a "higher is better" paradigm, so long as the temperature remains below degradation. Processing thermosetting polymer systems is more complex. Instead of the T_m^0 threshold, there exists one or more kinetic maxima for the thermosetting system at which the reaction proceeds at the fastest rate. Given the rapid thermal heating and decay cycles characteristic of L-PBF, we assume in this work that a kinetic maximum should be the target temperature affected by laser scanning. Affecting a temperature either below or above a kinetic maximum will limit the extent of reaction. Future work may exploit this phenomenon as a design consideration for targeting specific degrees of crosslinking or else varying the degree of crosslinking throughout the volume of the part. Equation 4 uses the generic T_x as the target temperature for crosslinking. In this work, the authors take $T_x = T_{x,peak}$ to target the maximum possible extent of crosslinking.

Results and Discussion

Predicted Process Parameter Range. The theoretical minimum energy density for maximum rate of reaction was determined according to the EXR (Equation 4) using the print parameter values from Table 1 and the measured material properties included in SI TABLE 1 as Supplemental Information. Figure 2 depicts the reaction rate as a function of temperature. Reaction rate is determined energetically by integrating the area under heat flow vs time data collected at various heating rates in DSC and normalizing the energy released at each timestep to the total energy evolved in the reaction. The temperature corresponding to the maximum rate of reaction is taken to be the target temperature for EXR calculation. The temperatures at maximum rate of reaction, resultant EXR material component, and theoretical maximum beam speed are presented in Table 2.

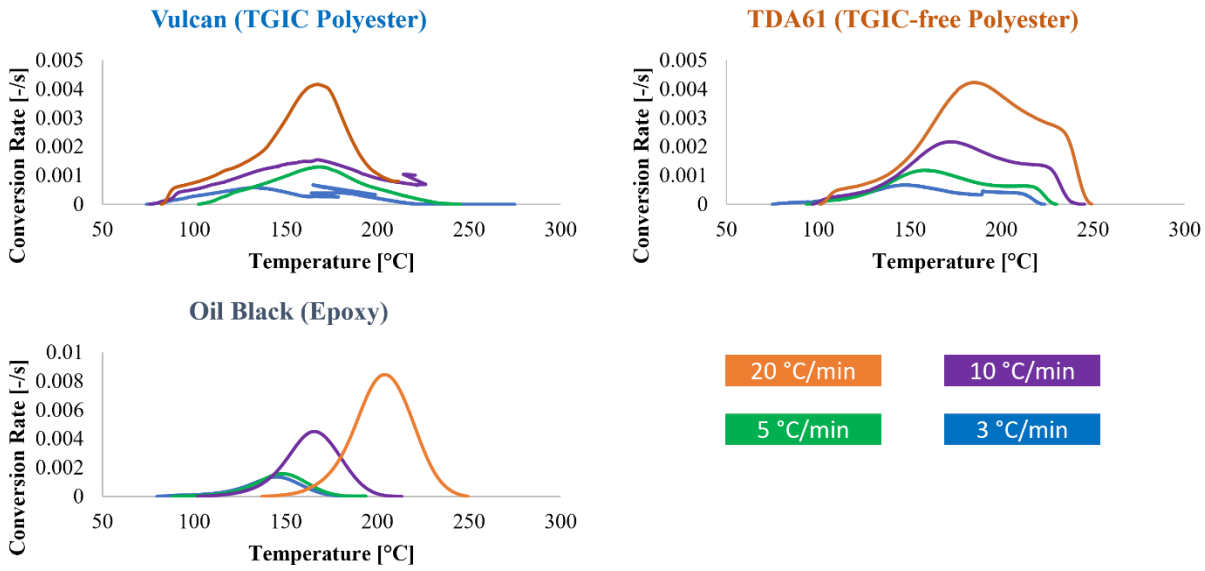

Figure 2. Rate of reaction (dα/dt) as a function of temperature at four heating rates for (a) Vulcan (TGIC polyester), (b) TDA61 (TGIC-free polyester), and (c) Oil Black (epoxy). Curves shown are the average of three replicate trials.

Table 2. Maximum theoretical beam speeds as predicted by EXR equation targeting the temperature for measured maximum rate of reaction for three thermosetting powder paints.

Material	dα/dt Peak [°C]	Initial Activation Energy [kJ mol^{-1}]	EXR_material [J mm^{-3}]	Maximum V_b [mm s^{-1}]
Vulcan (TGIC Polyester)	171	212	0.213	113
TDA61 (TGIC-free Polyester)	189	52	0.097	248
Oil Black (epoxy)	205	24	0.112	215

It should be noted that the initial activation energy reported in Table 2 is used to calculate EXR as the authors assume no reaction has occurred in the one-layer thick control volume. Figure 3 depicts the change in activation energy as a function of extent of reaction. Each of the three materials studied proceeds via different reaction mechanisms yielding different degrees of variance. Although initial activation energy is chosen for maximum beam speed calculation for the initially unreacted new layer, the energy requirements change over time. For a material like Vulcan (TGIC polyester), the activation energy is greatest for the unreacted state and significantly decreases as the reaction proceeds. This may result in reaching a higher temperature than desired if laser energy is not reduced as the reaction progresses. Conversely, TDA61 (TGIC-free polyester) increases the required activation energy with extent of reaction. This may result in a failure to achieve even a moderate extent of cure. The Oil Black (epoxy) material has an activation energy with the least variation, only increasing from 24 to 40 kJ mol^{-1} as the reaction progresses. A

material with an activation energy relationship like Vulcan (TGIC polyester) may be beneficial for L-PBF application as the high initial activation energy serves as a gatekeeper preventing unwanted reaction, but the lower activation energy to continue the reaction at higher extents of conversion may enable crosslinking to occur between layers where the available energy is lower than on the surface.

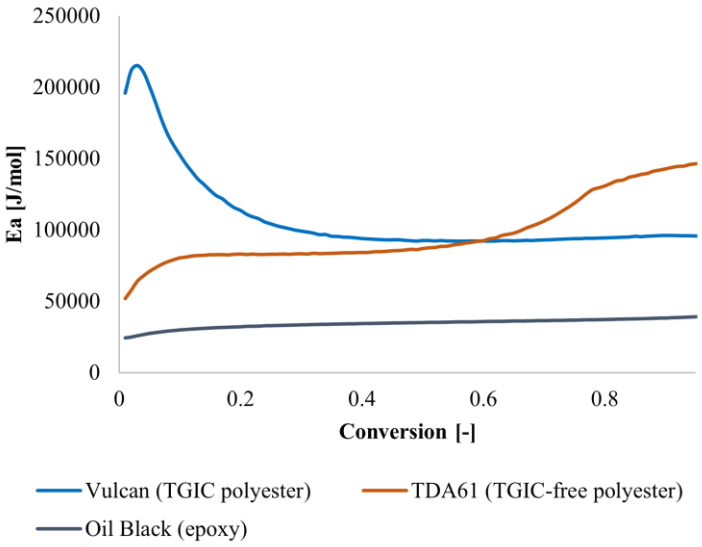

Figure 3. Activation energy as a function of conversion for three studied materials. A flat-line relationship would indicate a single-step reaction mechanism for curing, which is not observed for any of the studied materials. Instead, the data suggest complex multi-step reaction pathways for each material that are also different from each other.

The likely cause for activation energy increase in the TDA61 (TGIC-free polyester) is a kinetically limiting network morphology. At higher extents of conversion, more energy is required for molecules to diffusively move into available reaction sites. Such behavior likely also manifests as a reduction of powder coalescence rate at high extents of conversion. This topic should be explored in greater detail in future work.

Predicted and Measured Extent of Conversion. The temperature profiles collected at each process parameter value combination outlined in Table 1 were used to calculate extent of reaction according to Equation 5 and Equation 6. Equation 5 is calculated for values of α between 0.01 and 0.95 in steps of 0.01 using the model parameters *A, m,* and *n* determined from the fit of Equation 2. The resulting library of temperature- and conversion-dependent rate of reaction values are used in sequential evaluation of Equation 6 based on the experimentally collected *T(t)* data from the IR camera. In Equation 6, t_f is chosen to be the time at which $\alpha = \alpha_0 + 0.01$ (i.e., rate of reaction is assumed to be constant for each 0.01 conversion increment). A running calculation of α after each timestep *dt* yields the predicted conversion vs time plot, such as the representative plots included in .

$\frac{d\alpha}{dt}(T,\alpha)=A*exp\left(\frac{-E_A}{RT}\right)*\alpha^m*(1-\alpha)^n$	Equation 5
$\int_{t_0}^{t_f} \frac{d\alpha}{dt}(T(t))\,dt\,\vert_{\alpha=\alpha_0}$	Equation 6

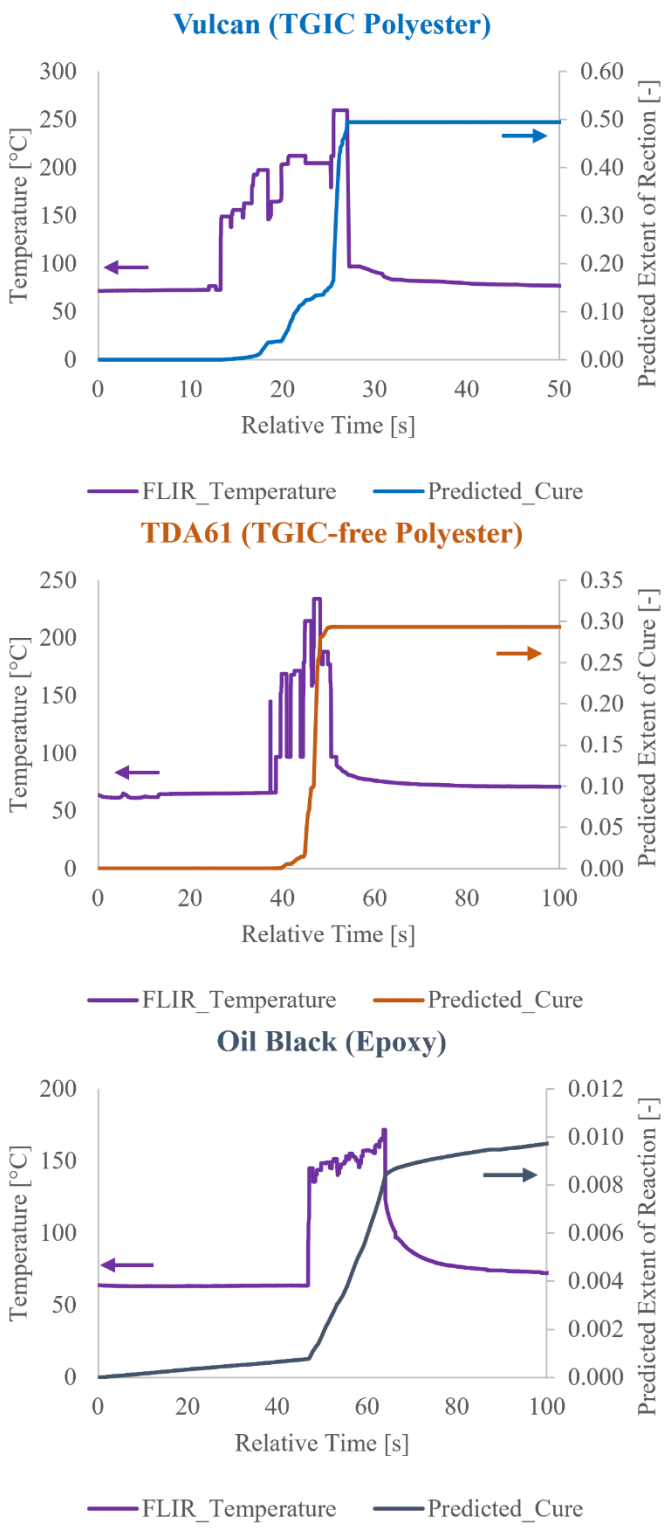

As the FLIR camera only measures surface temperature of the current layer, the predicted extent of cure is also only for a single layer. Any effects of reheating during laser scanning of subsequent layers are unaccounted for in the reported extent of conversion. It should be noted that the extent of conversion levels off as the laser leaves the region of interest and the local temperature cools rapidly to the chamber temperature. This indicates for the studied systems that curing only occurs during laser scanning, which is beneficial for maintaining geometric selectivity of reaction. These predictions are compared against extent of cure measured by DSC of parts printed at each process parameter value combination in Table 3. Looking over the data in Table 3, it is easy to notice the large variance of the reported maximum temperature. This variance cascades throughout both predicted and measured extent of cure. Although the authors have made the simplification assumptions of (i) constant distance between IR camera and every sample and (ii) a constant emissivity of 0.95, these would only effect the maximum temperature and predicted extent of conversion data columns. The high variance in the measured extent of cure data suggests that there is a naturally high variation in extent of reaction when cured via the rapid and cyclic heating characteristic of L-PBF. Despite the high variation, the authors discuss a few key abstractions for L-PBF printing thermosetting polymers in the following paragraphs.

Figure 4. Representative temperature profiles and resultant predicted cure profiles from Vulcan (TGIC polyester), TDA61 (TGIC-free polyester), and Oil Black (epoxy). Temperatures were collected via in situ FLIR camera at 70 °C bed temperatures and 40 mm s^{-1} beam speeds.

Table 3. Measured and predicted results of three studied materials at various process parameter value combinations.

Material	EXR = 1 Target Temperature [°C]	Beam Speed [mm s^{-1}]	Maximum Temperature [°C]	Predicted Extent of Cure (Isoconversional Model) [%]	Measured Extent of Cure (1-Hx/Hx0) [%]
Vulcan (TGIC Polyester)	171	20	302 ± 85	33 ± 52	13 ± 7
		40	260 ± 60	56 ± 17	34 ± 15
		60	178 ± 44	25 ± 35	13 ± 16
TDA61 (TGIC free polyester)	189	20	258 ± 51	94	1 ± 20
		40	234 ± 52	29	0.4 ± 10
		60	259 ± 62	32	4 ± 5
		150	153 ± 27	1 ± 1	8 ± 10
		235	124 ± 7	0.02 ± 0.005	19 ± 30
Oil Black (epoxy)	205	20	215 ± 51	2 ± 0.3	7 ± 4
		40	190 ± 27	0.9 ± 0.2	9 ± 2
		60	194 ± 49	0.8 ± 0.07	9 ± 1

As seen in Figure 5, there is the expected inverse relationship between scan speed and maximum temperature. However, the specific relationship between temperature and beam speed is material dependent. The observed results indicate that the material with highest initial activation energy (Vulcan, TGIC polyester) has the highest maximum temperature at slower scan speeds. The trend continues with Oil Black (epoxy) being the material with lowest initial activation energy and lowest maximum temperature at the slowest scan speeds studied. Additionally, the beam speeds required to achieve the target temperatures and predicted EXR values from Table 2 and significantly slower than predicted by the EXR's energy balance. All three studied materials required more energy (i.e., slower beam speed) than theoretically predicted to achieve the desired temperature for maximum rate of reaction. One assumption of the original EMR that is carried over into the current form of the EXR is 100% efficient conversion of laser energy into thermal energy. It is likely that this is a poor assumption for the 455 nm UV diode laser used in the present work.

The Vulcan (TGIC polyester) was observed to reach the highest extent of cure during L-PBF printing, as determined by post-print DSC. This is unsurprising given that the Vulcan material was observed to both reach the highest maximum temperature of the three materials at a given beam speed, and Vulcan is the only studied material to decrease activation energy as a function of

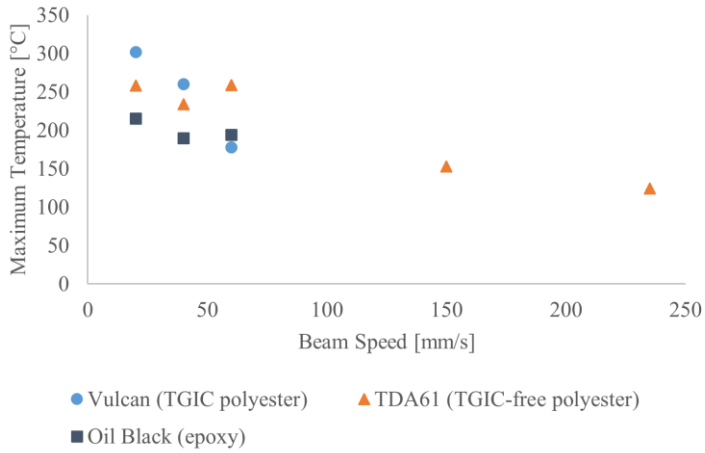

Figure 5. Relationship between average maximum temperature and scan speed for the three materials studied.

extent of reaction (See Figure 3). The exact contributions of each phenomenon are, however, convoluted.

The Oil Black (epoxy) material is the only one where the isoconversional model underpredicts the extent of cure. Both the underprediction of the Oil Black material and overprediction of the TDA61 and Vulcan materials can be explained by the isoconversional verification plots shown in Figure 6. The modeled rate of reaction (solid line) for Oil Black is consistently lower than the measured rate of reaction (x's); the opposite is true for both Vulcan (TGIC polyester) and TDA61 (TGIC-free polyester). This is especially true at 20 °C min^{-1}, the fastest heating rate used in this study. Given that the rates observed by IR camera are on the order of 40 °C min^{-1}, one might expect the actual deviation from the model to be even greater.

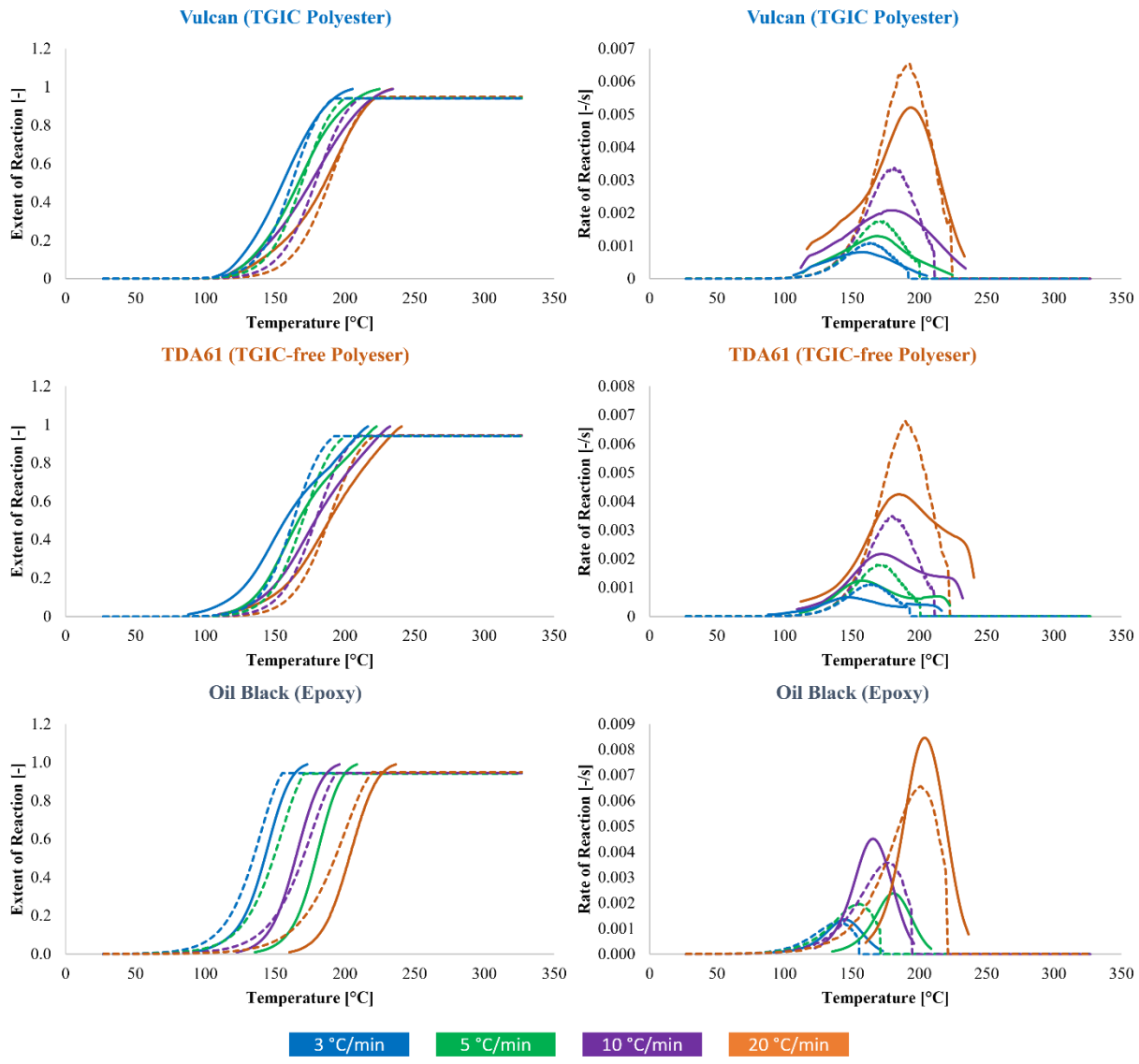

Figure 6. Representative isoconversional model fit validation curves for (a) Vulcan (TGIC polyester), (b) TDA61 (TGIC-free polyester), and (c) Oil Black (epoxy). Solid lines represent measured data and dashed lines represent fitted data.

Summary and Future Work

Work presented in this manuscript centers on closing the gap for fabricating a covalent networked polymer during the laser powder bed fusion additive manufacturing processing. The equations used for theoretical determination of process parameter values were expanded from their original forms that only included considerations of thermoplastic polymer process to include activation energy and acknowledge the temperature of maximum rate of reaction. Parameter values were predicted via the new form of the Energy Melt Ratio equation, termed Energy Reaction Ratio (EXR), for three thermosetting polymer systems, each employing unique curing mechanisms, never-before fabricated via L-PBF and the resulting processability was assessed.

Temperature profiles from parameter value combinations above the predicted threshold were measured using an *in situ* infrared camera. Extent of reaction was predicted using an isoconversional kinetic model from the collected thermal profiles. The post-print extent of reaction measurements via DSC revealed poor agreement with the isoconversionally predicted values. Potential sources of error from measurements and model assumptions were discussed. One major concern is the degree of variation in measured temperature profiles. Future work should include an investigation in bed location dependence and scan order on maximum temperature measured. Although its size and price point make the Sintratec Kit well-suited for material development research, there are L-PBF printers (including other models from Sintratec) with more sophisticated hardware and software to ensure greater repeatability across the build platform, across layers, and across builds. Perhaps the observed temperature variation is truly a function of the interactions between the UV diode laser and studied materials. Further investigations of the same polymer systems on different L-PBF machines are required to distinguish the effects of hardware and materials from each other.

There is additional opportunity to improve the isoconversional model. As evidenced by the fit data in Figure 6, the assumptions of using only one autocatalytic and one non-autocatalytic term in the model do not accurately represent the two polyester systems studied (i.e., Vulcan and TDA61). A more robust model would include, at a minimum, a diffusive term, as the authors hypothesize this accounts for the increase in activation energy as a function of conversion for the TDA61 (TGIC-free polyester) system. Current COTS thermosetting systems designed for other manufacturing methods are often complex, multi-step reactions. We should expect future thermosetting systems designed for L-PBF processing to be equally or more complex, given the local, rapid, and layerwise cyclical thermal cycles characteristic of L-PBF.

A second means of potentially improving the isoconversional predictions is to use heating rates closer to those observed in L-PBF processing when determining the kinetic triplet. Data can be collected at such heating rates using fast calorimetry (e.g., Mettler Toledo's Flash DSC).

Future work should investigate the effect of various laser wavelengths on the extent of reaction achieved during L-PBF. It is very likely that L-PBF processing of thermosetting systems will have a higher degree of wavelength dependency than thermoplastic polymers. The additional concerns of activation energy for chemical reaction and the kinetic maximum target temperature have an increased opportunity for energy selectivity over the purely physical changes occurring during thermoplastic processing. This would be especially true when including an initiator species into the resin mixture, such as is common in vat photopolymerization AM.

The future of thermosetting polymers in L-PBF hinges on the availability of powdered feedstock, which is also a concern for thermoplastic polymer L-PBF. The current work focused on COTS material available as a powder. Most polymer processing techniques, for both thermosetting and thermoplastic polymers, do not use a powdered feedstock form. As discussed elsewhere [2], recoating requirements for L-PBF are specific and powder production is significantly more complex than, for example, converting readily available pellets into filament for FFF AM. The significant challenge of feedstock form must be addressed for L-PBF to reach its full impact.

Acknowledgements

The authors would like to acknowledge R. Chandler Hawsey at SRNL for his assistance in DSC sample preparation and data collection. Funding for this work was provided by the NNSA Additive Coordination Team (ACT), an NA-115 driven partnership to enable additive manufacturing solutions for enterprise needs.

References

[1] ASTM, *Additive Manufacturing - General Principles - Fundamentals and Vocabulary,* ISO/ASTM, 2021.

[2] C. A. Chatham, T. E. Long and C. B. Williams, "A review of the process physics and material screening methods for polymer powder bed fusion additive manufacturing," *Progress in Polymer Science,* vol. 93, pp. 68-95, 2019.

[3] R. Goodridge, C. Tuck and R. Hague, "Laser sintering of polyamides and other polymers," *Progress in Material Sciecne,* vol. 57, no. 2, pp. 229-267, 2012.

[4] A. Das, C. A. Chatham, J. J. Fallon, C. E. Zawaski, E. L. Gilmer, C. B. Williams and M. J. Bortner, "Current understanding and challenges in high temperature additive manufacturing of engineering thermoplastic polymers," *Additive Manufacturing,* vol. 34, p. 101218, 2020.

[5] L. Tan, W. Zhu and K. Zhou, "Recent progress on polymer materials for additive manufacturing," *Advanced Functional Materials,* vol. 30, p. 2003062, 2020.

[6] S. Sun, G. Fei, X. Wang, M. Xie, Q. Guo, D. Fu, Z. Wang, H. Wang, G. Luo and H. Xia, "Covalent adaptable networks of polydimethylsiloxane elastomer for selective lasr sintering 3D printing," *Chemical Engineering Journal,* vol. 412, p. 128675, 2021.

[7] S. Sun, X. Gan, Z. Wang, D. Fu, W. Pu and H. Xia, "Dynamic healable polyurethane for selective laser sintering," *Additive Manufacturing,* vol. 33, p. 101176, 2020.

[8] K. C. Chuang, T. Gornet and H. Koerner, "Challenges in Laser Sintering of Melt-Processable Thermoset Imide Resin," NASA, 2016.

[9] K. C. Chuang, T. J. Gornet, K. Schneidau and H. Koerner, "Determining if laser sintering can be applied to high-temperature thermoset polyimides to enhance covalent bonding between layers through the curing of the reactive endcaps, as compared to conventional thermoplastic polymers that display poor z-directiona," Thermal Processing, 2020.

[10] M. S. Hassan, K. M. M. Billah, S. E. Hall, S. Sepulveda, J. E. Regis, C. Marquez, S. Cordova, J. Whitaker, T. Robison, J. Keating, E. Shafirovich and Y. Lin, "Selective laser

sintering of high-temperature thermoset polymer," *Journal of Composite Science,* vol. 6, no. 41, 2022.

[11] C. G. Campbell, D. J. Astorga, E. Martinez and M. Celina, "Selective laser sintering (SLS)-printable thermosetting resins via controlled conversion," *MRS Communications,* 2021.

[12] D. Lascano, A. Lerma-Canto, V. Fombuena, R. Balart and N. Montanes, "Kinetic analysis of the curing process of biobased epoxy resin from epoxidized linseed oil by dynamic differential scanning calorimetry," *Polymers,* vol. 13, p. 1279, 2021.

[13] T. L. Starr, T. J. Gornet and J. S. Usher, "The effect of process conditions on mechanical properties of laser-sintered nylon," *Rapid Prototyping Journal,* vol. 17, pp. 418-423, 2011.

[14] M. Vasquez, B. Haworth and N. Hopkinson, "Optimum sintering region for laser sintered nylon-12," *Proceedings of the Institution of Mechanical Engineers, Part B: Journal of Engineering Manufacture,* vol. 225, pp. 2240-2248, 2011.

[15] C. A. Chatham, T. E. Long and C. B. Williams, "Powder bed fusion of poly(phenylene sulfide) at bed temperatures significantly below melting," *Additive Manufacturing,* vol. 28, pp. 506-516, 2019.

SUPPLEMENTAL INFORMATION

SI TABLE 1. Manufacturer recommended curing parameters and material properties for each studied material. Column headers marked with an asterisk indicate properties measured by the authors.

Material	Oven Temperature [°C]	OEM recommended Dwell Time [min]	Cp* [J $g^{-1}K^{-1}$]	Density [g cm^{-3}]	$T_{x,peak}$* [°C]	ΔHm* [J g^{-1}]
Vulcan Black (TGIC Polyester)	200	10	1.7	1.63	171	6.06
Oil Black (Epoxy)	130-200	4-13+	1.5	1.35	205	9.72
TD 61 (TGIC free polyester)	180-200	6-25	1.4	1.2	189	7.51

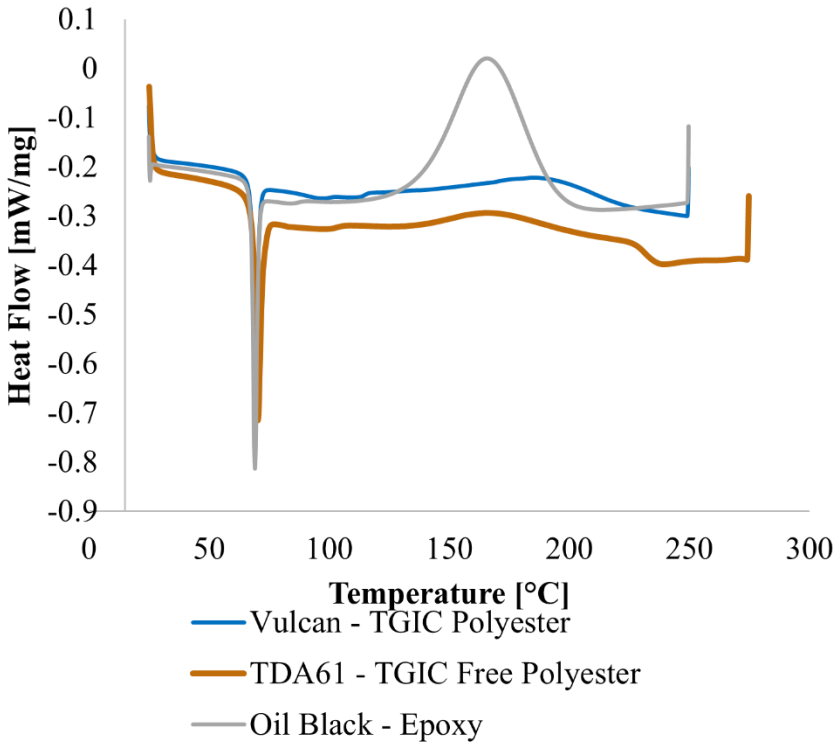

SI FIGURE 1 Representative first heat DSC curves for three studied materials. Curves are plotted exotherm up and data were collected at a heating rate of 10 °C min^{-1}.

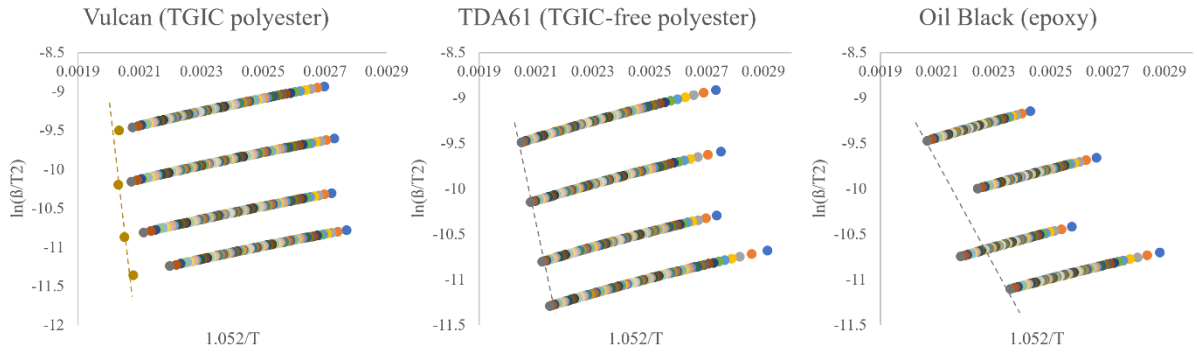

SI FIGURE 2. Kissinger linear fits for determining activation energy as a function of each constant value of conversion [0.01-0.95]. Dashed line guides the eye for an example set of four datapoints from different heating rates at the same degree of conversion.